Pore-forming toxin-mediated ion dysregulation leads to death receptor-independent necroptosis of lung epithelial cells during bacterial pneumonia

Norberto González-Juarbe[1], Kelley Margaret Bradley[1], Anukul Taranath Shenoy[1], Ryan Paul Gilley[2], Luis Felipe Reyes[3], Cecilia Anahí Hinojosa[3], Marcos Ignacio Restrepo[3,4], Peter Herman Dube[2], Molly Ann Bergman[2,5] and Carlos Javier Orihuela*,[1,2]

We report that pore-forming toxins (PFTs) induce respiratory epithelial cell necroptosis independently of death receptor signaling during bacterial pneumonia. Instead, necroptosis was activated as a result of ion dysregulation arising from membrane permeabilization. PFT-induced necroptosis required RIP1, RIP3 and MLKL, and could be induced in the absence or inhibition of TNFR1, TNFR2 and TLR4 signaling. We detected activated MLKL in the lungs from mice and nonhuman primates experiencing *Serratia marcescens* and *Streptococcus pneumoniae* pneumonia, respectively. We subsequently identified calcium influx and potassium efflux as the key initiating signals responsible for necroptosis; also that mitochondrial damage was not required for necroptosis activation but was exacerbated by MLKL activation. PFT-induced necroptosis in respiratory epithelial cells did not involve CamKII or reactive oxygen species. KO mice deficient in MLKL or RIP3 had increased survival and reduced pulmonary injury during *S. marcescens* pneumonia. Our results establish necroptosis as a major cell death pathway active during bacterial pneumonia and that necroptosis can occur without death receptor signaling.

It is estimated that 450 million individuals develop pneumonia annually.[1] Those most susceptible for respiratory tract infections are infants and the elderly with pneumonia ranked as the eighth leading cause of death worldwide.[2] During bacterial pneumonia, most pathogens release cytotoxic products that are capable of killing respiratory cells. Principal among these are pore-forming toxins (PFTs), the most common cytotoxic product produced by pathogenic bacteria.[3–5] PFTs target eukaryotic cell membranes and at high concentrations form lytic pores. At lower concentrations, pores caused by PFTs result in ion dysregulation, disruption of cell signaling and function, and in some instances apoptotic or pyroptotic death.[6] At the gross level, PFTs have been implicated in immune cell depletion, pulmonary damage, vascular leakage, consolidation of the alveoli and development of acute respiratory distress syndrome.[7–12] Importantly, and despite decades of research, the molecular basis for how PFTs kill host cells continues to be elucidated.[5]

Necroptosis is a pro-inflammatory cell death program that is caspase-independent. Similar to pyroptosis, but without activation of the inflammasome, it results in cell membrane rupture and the release of cytoplasmic components that act as alarmins. Necroptosis was originally observed *in vitro* when stimulation of Fas/CD95 or tumor necrosis factor receptor 1 (TNFR1) occurred simultaneously to inhibition of caspase activation with the pan-caspase inhibitor Z-VAD-FMK.[13–15]

Today, necroptosis is considered to be central in the generation of an immune response in tissues following sterile injury, such as an ischemic episode.[16] Necroptosis is also understood to contribute to the persistent inflammation that is observed in many chronic diseases such as cancer and atherosclerosis.[17]

During necroptosis, engagement of TNFR1 by tumor necrosis factor (TNF) leads to the formation of a membrane-bound complex containing TNFR1, the adaptor protein TRADD and the receptor interacting protein kinase (RIP)1 (i.e., complex I). Subsequently, and only when caspase-8 is inhibited, the adaptor protein FADD is recruited to cytoplasmic complex II (consisting of TRADD, TRAF2, RIP1, FADD, pro-caspase-8 and FLIP) and this leads to the activation of RIP3 and its substrate the mixed-lineage kinase domain-like protein (MLKL).[18,19] Phosphorylated MLKL (pMLKL) is the effector of necroptosis and translocates to cellular membranes to induce their dissolution and the release of intracellular contents.[20–24] Toll-like receptor (TLR)4 and TLR3 signaling also activates necroptosis when caspases are inhibited.[25–27] This occurs in a TRIF-, RIP1-, RIP3- and MLKL-dependent manner.[18] Likewise, DAI (also known as ZBP1/DLM-1) has been shown to detect intracellular dsRNA and activate RIP3 in virus-infected cells.[28,29] Most recently, necroptosis has been shown to involve the activation of calmodulin-dependent protein kinase II (CamKII) by RIP3, the latter occurs in response to reactive

[1]Department of Microbiology, The University of Alabama at Birmingham, 845 19th Street South, Birmingham, AL 35294-2170, USA; [2]Department of Microbiology and Immunology, The University of Texas Health Science Center at San Antonio, 8403 Floyd Curl Drive, San Antonio, TX 78229, USA; [3]Division of Pulmonary Diseases and Critical Care Medicine, Department of Medicine, The University of Texas Health Science Center at San Antonio, San Antonio, TX 78229, USA and [4]Division of Pulmonary Diseases and Critical Care Medicine, South Texas Veterans Health Care System, San Antonio, TX 78229, USA
*Corresponding author: CJ Orihuela, Department of Microbiology, The University of Alabama at Birmingham, 845 19th Street South, Birmingham, AL 35294-2170, USA. Tel: +205-975-2536; Fax: +205 996 4008; E-mail: corihuel@uab.edu
[5]Current address: Belmont, MA 02478, USA.

oxygen species (ROS)-mediated injury[30] and ROS-mediated intracellular Ca^{++} alterations.[31] Thus, necroptosis is primarily thought to be a death receptor-dependent form of inflammatory cell death, albeit pathogen recognition receptors and other sensors of intracellular damage are increasingly being implicated.

In the past few years, a considerable body of evidence has emerged showing that necroptosis has mixed but highly important roles in the airway during pneumonia. In a mouse model of Influenza A infection, blocking of RIP3 activity increased viral titers and worsened disease outcomes.[32] Both murine cytomegalovirus and herpes simplex virus were shown to block necroptosis, thus enabling the development of mature viral particles.[33] The current consensus indicates that necroptosis is protective during viral pneumonia and a way for infected lung cells to abort viral replication.[18] In stark contrast, necroptosis is detrimental during bacterial pneumonia. Our laboratory has shown that bacterial PFTs cause a rapid and necroptosis-dependent depletion of alveolar macrophages and this worsened outcomes.[8,34] Our group and Kitur *et al*.[35] have also shown that treatment of mice with necroptosis inhibitors substantially reduced pulmonary injury during *Serratia marcescens* (*Sma*) or Staphylococcal pneumonia, respectively, and this was PFT-dependent.[8] Importantly, other than alveolar macrophages, no other lung cell type has been specifically examined to learn the impact of necroptosis during bacterial pneumonia.

Herein, we report for the first time that PFT-producing bacteria and purified PFTs induce respiratory epithelial cell necroptosis. Contrary to other systems where necroptosis becomes engaged as a result of death receptor signaling, we report that RIP1/RIP3/MLKL activation following PFT exposure is instead the result of Ca^{++} and K^{+} dysregulation that occurs following PFT-induced membrane damage. Our results suggest necroptosis may occur under a broader context of cellular insults, expand our molecular understanding of bacterial pathogenesis and programmed cell death, and add to the existing body of evidence that suggest blocking necroptosis is a way to protect against injury during bacterial infection. Our studies also establish PFTs as an important molecular tool for the study of necroptosis as no caspase inhibition was required.

Results

PFTs induce tissue damage and death of respiratory epithelium. *Sma* is a Gram-negative opportunistic pathogen that secretes a 165 kDa PFT called ShlA. The latter is responsible for the hemorrhagic phenotype observed during *Sma* pneumonia.[8] Other PFTs that are significant contributors to tissue damage during bacterial pneumonia include *Streptococcus pneumoniae* (*Spn*) pneumolysin, a cholesterol-dependent cytolysin, and *Staphylococcus aureus* α-toxin.[35–38]

As evidence for the former, the lungs from mice infected intratracheally with *Sma* demonstrated edema, lung consolidation, hemorrhage and the presence of cellular debris. These pathological hallmarks were absent in the lungs collected from mice challenged with an isogenic ShlA-deficient mutant (Δ*shlA*; Figure 1a). Mice infected with Δ*shlA* also had

significantly less albumin (Figure 1b), a marker of vascular leakage, and lactate dehydrogenase (Figure 1c), a marker of cell death, present within isolated bronchoalveolar lavage fluid (BALF). Similar results were observed in mice intratracheally challenged with recombinant pneumolysin (rPly) but not with the heat inactivated control (HI-rPly; Supplementary Figure 1). *In vitro*, death of A549 human type II pneumocytes and LA-4 mouse bronchial epithelial cells was also found to be ShlA-dependent (Figure 1d) and pneumolysin-dependent (Figure 1e) following infection with the corresponding pathogen and its isogenic mutant. Together, these results highlight the major role of PFTs in mediating acute lung injury during bacterial pneumonia.
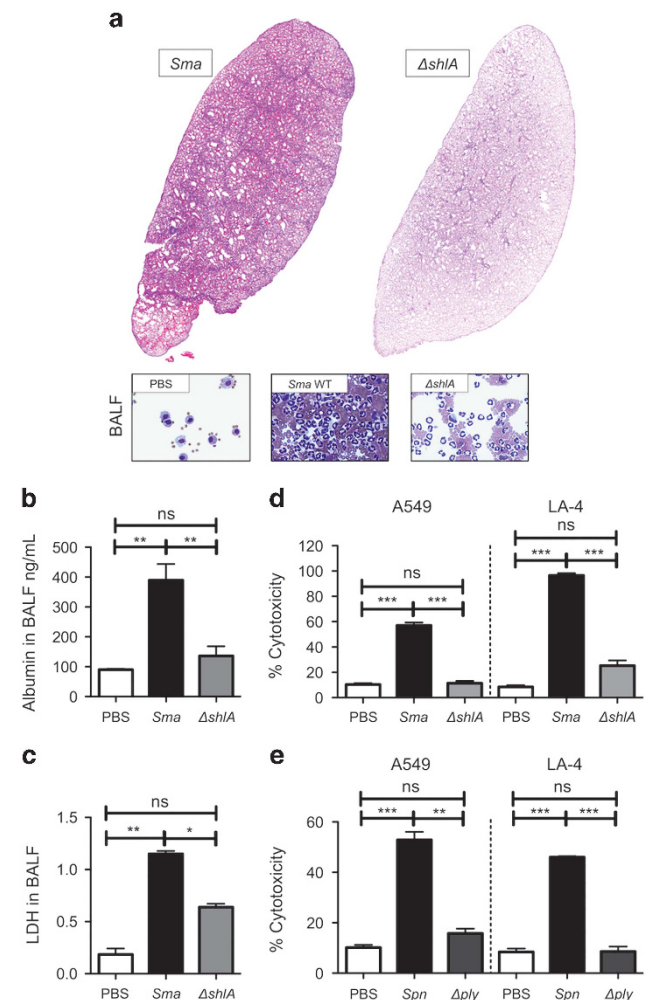

Figure 1 *Sma* induces pore-forming toxin-dependent tissue damage and respiratory epithelial cell death. C57BL/6 mice (four to six per cohort) were challenged intratracheally with 5.0×10^6 CFU of *S. marcescens (Sma)* or an isogenic ShlA-deficient mutant (Δ*shlA*). Infected mice were killed at 24 h post-infection for (**a**) pathological evaluation of their lungs and BALF, and determination of (**b**) albumin and (**c**) lactate dehydrogenase (LDH) levels in BALF. Percent cytotoxicity measured by LDH release for A549 human type II pneumocytes and LA-4 mouse bronchial epithelial cells infected with (**d**) *Sma* or Δ*shlA* at MOI 10, alternatively (**e**) *S. pneumoniae (Spn)* or an isogenic mutant deficient in pneumolysin (Δ*ply*) at MOI 100. Mann–Whitney *U*-tests were applied for two-group comparisons: $*P < 0.05$, $**P \leqslant 0.01$, $***P \leqslant 0.001$. *In vitro* assays show the averaged value from more than three separate experiments
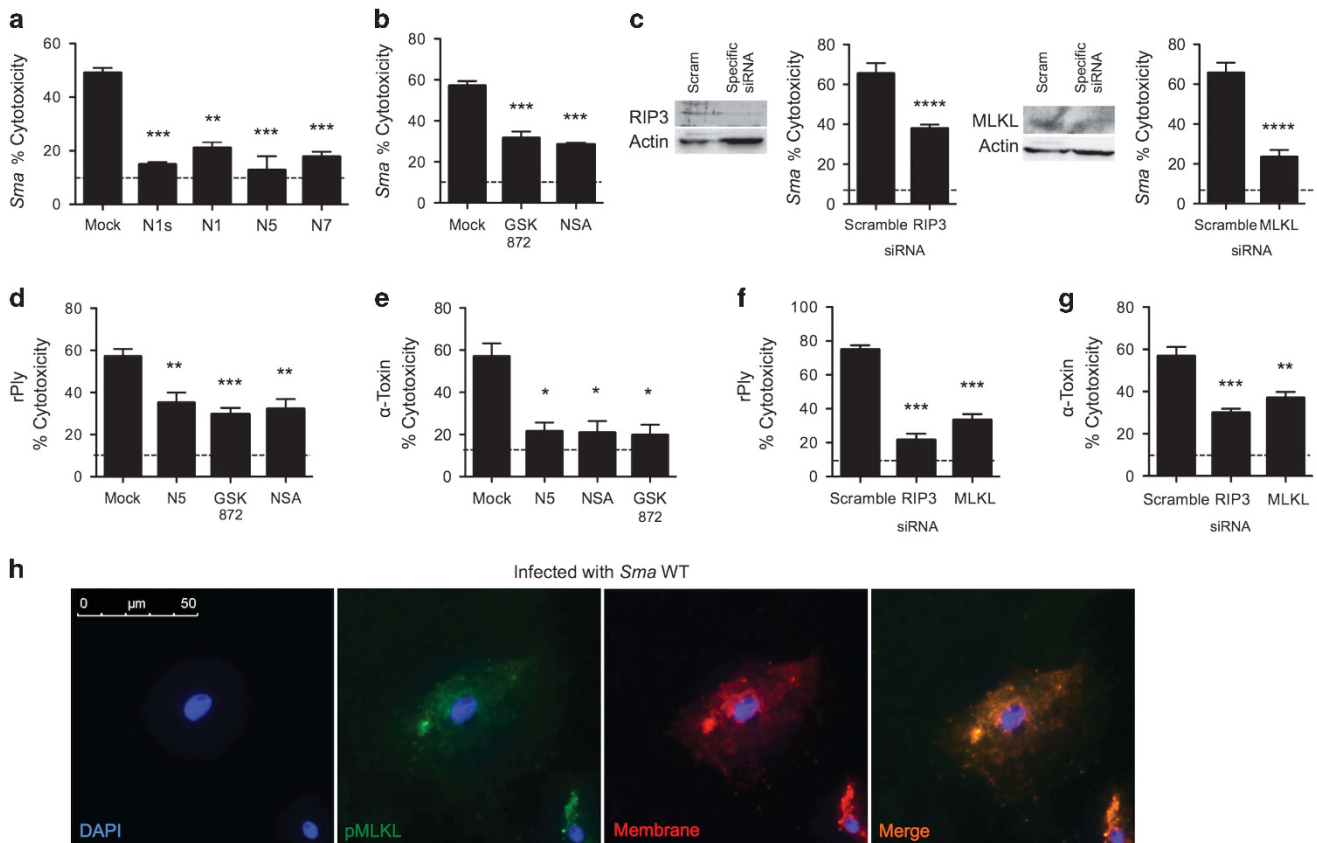
Figure 2 Pore-forming toxins cause respiratory epithelial cell necroptosis. Percent cytotoxicity as measured by LDH assay of *S. marcescens*-infected (MOI 10) A549 cells pretreated with (**a**) RIP1 inhibitors necrostatin-1 s (N1s, 10 μM), necrostatin-1 (N1, 10 μM), necrostatin-5 (N5, 10 μM), necrostatin-7 (N7, 10 μM), (**b**) the RIP3 inhibitor GSK' 872 (10 μM), the MLKL inhibitor necrosulfonamide (NSA; 10 μM), or mock-treated with media containing an equivalent DMSO concentration. (**c**) Immunoblots for RIP3 and MLKL and corresponding percent cytotoxicity of *S. marcescens*-infected A549 cells transfected with siRNA against RIP3 and MLKL. Percent cytotoxicity of (**d**) pneumolysin (rPly: 0.32 μg/ml) or (**e**) α-toxin (3.9 μg/ml) challenged A549 cells pretreated with Nec-5, GSK' 872, NSA or mock-treated. Percent cytotoxicity of (**f**) rPly and (**g**) α-toxin challenged A549 cells transfected with siRNA against RIP3, MLKL or a scrambled control. (**h**) Immunofluorescent staining of a *S. marcescens*-infected A549 cell. Cell nucleus (DAPI, blue), phosphorylated MLKL (pMLKL, green), cellular membrane (red, Dil cellular membrane label, Emission: 565 nm), Merge (orange). Mann–Whitney *U*-test was used for two-group comparisons. For multi-group comparisons, Dunn's multiple-comparison post-test was used: $*P < 0.05$, $**P \leqslant 0.01$, $***P \leqslant 0.001$. The mean value for *in vitro* experiments was averaged from more than three separate experiments. Dotted lines in panels indicate the average LDH level detected in supernatants of uninfected controls

Pore-forming toxins trigger alveolar epithelial cell necroptosis *in vitro*. To directly test whether PFTs killed lung epithelial cells via necroptosis, A549 cells were pretreated with inhibitors or siRNA targeting various points in the necroptosis pathway and then challenged with bacteria or purified PFTs. Pharmacological inhibitors of RIP1 (Figure 2a), RIP3 and MLKL (Figure 2b), all conferred protection against *Sma*-induced death. Similarly, siRNA knockdown of RIP3 and MLKL conferred protection against *Sma* challenge (Figure 2c). Our efforts to purify active recombinant ShlA were unsuccessful; instead we tested the specific role for purified rPly and *α*-toxin. Both PFTs induced A549 cell death that could be blocked with chemical inhibitors of RIP1, RIP3 and MLKL (Figures 2d and e). The treatment of cells with siRNA to knock down RIP3 and MLKL also protected against purified PFT-induced cell death (Figures 2f and g). Moreover, using immunofluorescent microscopy, we detected phosphorylated MLKL (pMLKL), at the plasma membrane of *Sma*-infected A549 cells (Figure 2h). Of note, diverse PFT-producing bacteria

including *Spn*, *S. aureus*, *Listeria monocytogenes* and uropathogenic *Escherichia coli*, also caused RIP1-dependent death in A549 cells (Supplementary Figure 2). Moreover, pharmacological inhibition and siRNA knockdown of caspase-1 did not protect A549 cells against *Sma* or rPly-induced death (Supplementary Fig S3), thereby ruling out caspase-1-dependent pyroptosis. Collectively, these results establish necroptosis as a principal cause of lung cell death following exposure to a PFT.

Necroptosis occurs in the lungs of mice and nonhuman primates experiencing severe pneumonia. Supporting an important role for necroptosis *in vivo*, we observed an increase in total airway levels of MLKL and pMLKL during development of sublethal *Sma* pneumonia in mice and their subsequent decrease during resolution (Figure 3a). Immunofluorescent (IF) and immunohistochemical staining for pMLKL prominently localized the protein to the bronchial epithelium of *Sma*-infected mouse lung sections, although pMLKL was also detected throughout the parenchyma (Figure 3b). We
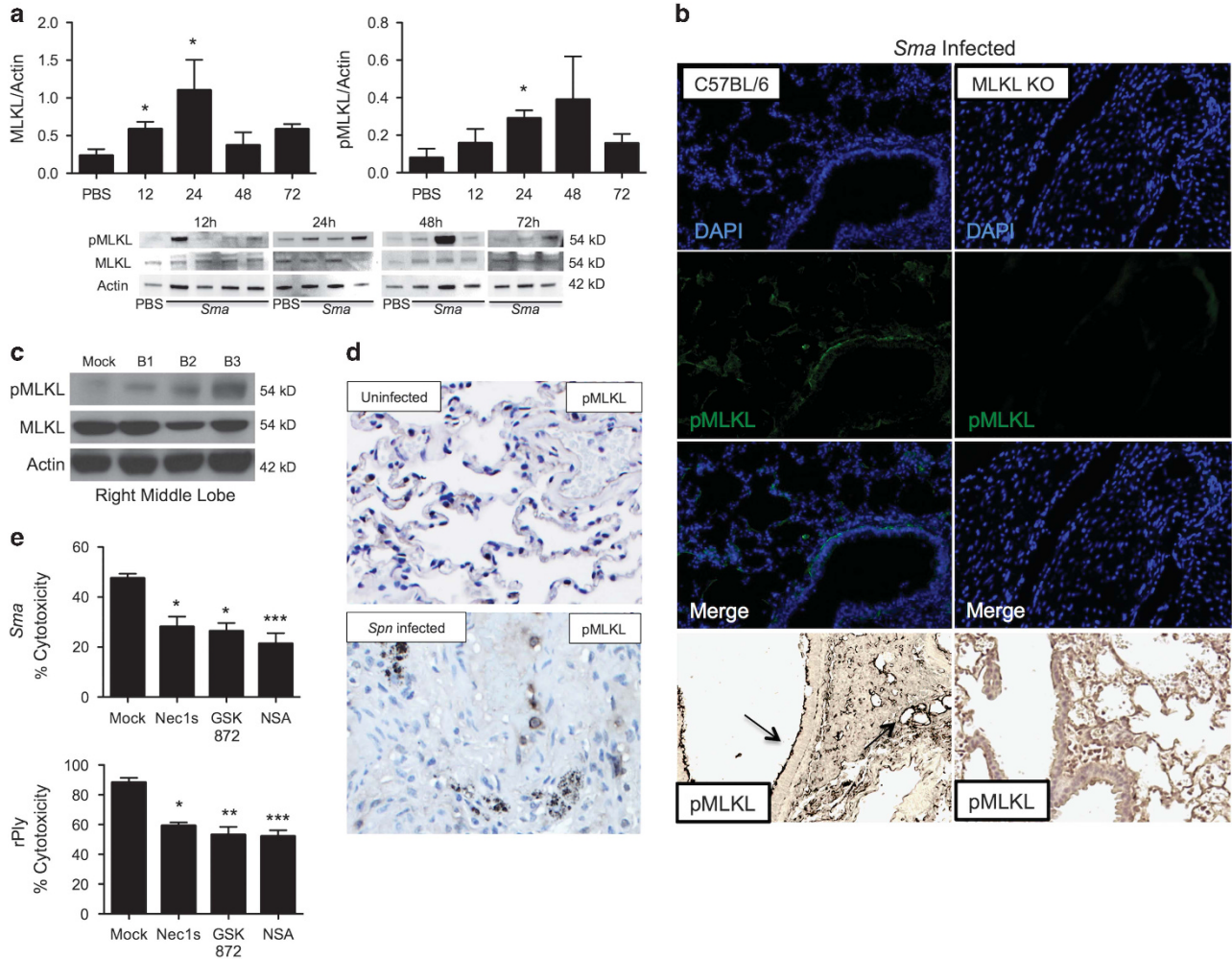
Figure 3 MLKL is active in murine and nonhuman primate respiratory epithelium during severe bacterial pneumonia. (**a**) Eight-week-old C57BL/6 mice (six to nine mice per cohort) were infected intratracheally with *S. marcescens* and killed at 4, 12, 24, 48 and 72 h post-infection for immunoblots for MLKL and pMLKL and its quantification. Relative levels in protein expression were determined by comparing the ratio of the detected band *versus* total protein levels as determined using Image J software. (**c**) IF and Immunohistochemistry of lung sections stained for pMLKL. Healthy baboons were challenged intrabronchially with *Spn* using a video-assisted bronchoscope and killed 5–7 days after infection for tissue collection. (**c**) Immunoblot for MLKL, pMLKL and actin (loading control) in the right middle lobe and left upper lobe of infected baboons *versus* uninfected control. (**d**) IHC for pMLKL (images taken at ×200). Primate data are from three infected baboons (B1–3) and an uninfected control (mock). (**e**) Percent cytotoxicity of *Sma*-infected (MOI 10) or pneumolysin (rPly: 0.32 μg/ml) challenged normal human primary epithelial cells pretreated with RIP1 inhibitor necrostatin-1 s (N1s, 10 μM), the RIP3 inhibitor GSK' 872 (10 μM) and the MLKL inhibitor necrosulfonamide (NSA; 10 μM), or mock-treated with media containing an equivalent DMSO concentration. For multi-group comparisons, Dunn's multiple-comparison post-test was used: *$P < 0.05$, **$P \leqslant 0.01$, ***$P \leqslant 0.001$. The mean value for *in vitro* experiments was averaged from more than three separate experiments

also observed elevated pMLKL levels in lung samples from nonhuman primates, that is, baboons, with experimental pneumococcal pneumonia (Figure 3c). Immunohistochemistry also showed widespread staining for pMLKL throughout the consolidated lungs of infected baboons (Figure 3d). Finally and importantly, pretreatment of primary normal human bronchial epithelial cells with inhibitors of RIP1, RIP3 and MLKL protected against cell death *in vitro* caused by *Sma* and rPly (Figure 3e). Thus, our collective results indicate that lung epithelial cell necroptosis occurs during Gram-negative and Gram-positive bacterial pneumonia, it is triggered by PFTs and this is conserved across a wide range of mammalian species.

PFT-induced respiratory cell necroptosis is independent of TNFR signaling and TLR4. As indicated, TNFR1 or TLR4 signaling during caspase-8 inhibition can lead to activation of the necroptosis pathway.[18] Pretreatment of cells with SPD304, which inhibits TNF-α trimerization and recognition by TNFR1,[39] or with R7050, which blocks TNFR1 association with TRADD and RIP1,[40] did not confer protection against *Sma*- or rPly-induced A549 death (Figure 4a), or death of normal human primary bronchial epithelial cells (Supplementary Figure 4). Furthermore, mice lacking TNFR1/TNFR2 (TNFR1/2 KO) had equivalent *Sma* burden and levels of LDH and albumin in isolated BALF as did wild-type controls (Figures 4b–e). Lung pathology also showed no discernable
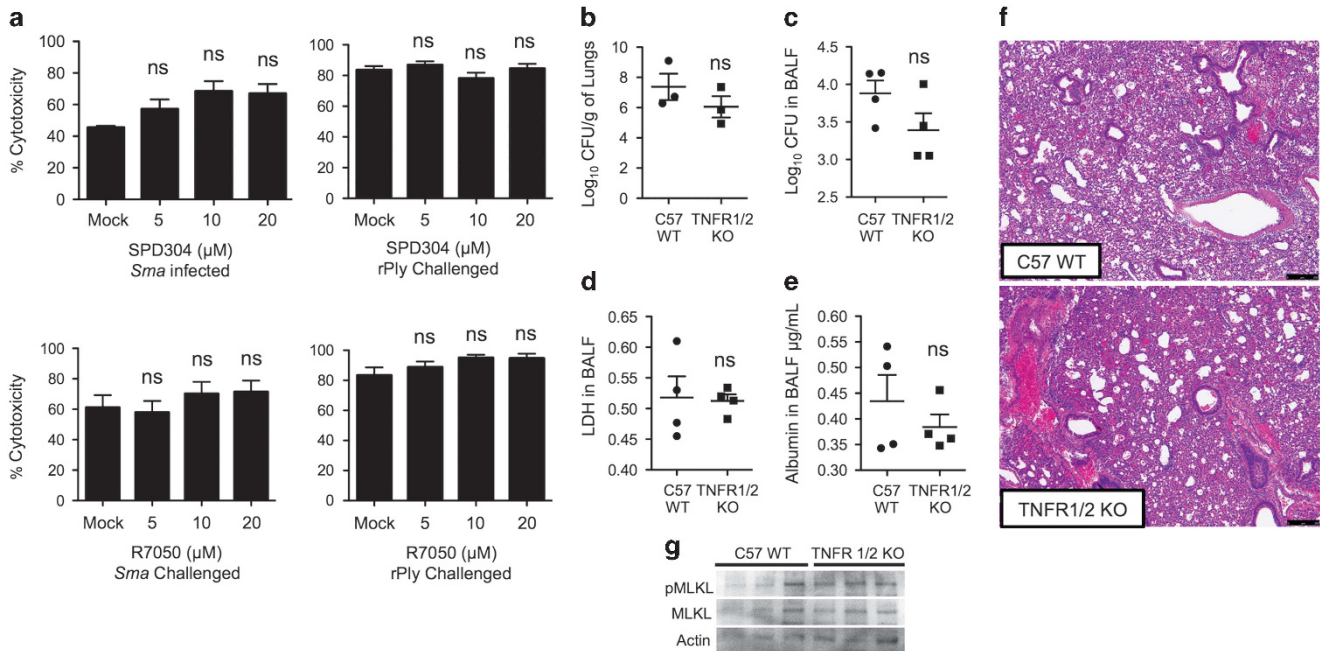
Figure 4 TNF-α or TNFR inhibition does not protect against PFT-mediated respiratory epithelial cell necroptosis. (**a**) Percent cytotoxicity of A549 cells infected with *Sma* or challenged with rPly pretreated with a small inhibitor of TNF-α (SPD304) or a selective inhibitor of TNFR1 (R7050) as determined using an LDH assay. (**b–g**) TNFR KO mice and wild-type controls of same age (five to seven mice per cohort) were infected intratracheally with *S. marcescens*. After 24 h, levels of (**b**) bacterial titers in lungs and (**c**) BALF, (**d**) LDH and (**e**) albumin were determined. (**f**) H and E staining of lung tissue. (**g**) Immunoblots for pMLKL and MLKL in lung tissue. Mann–Whitney *U*-test was used for two-group comparisons. For multi-group comparisons, Dunn's multiple-comparison post-test was used: NS denotes no significance. The mean value for *in vitro* experiments was averaged from more than three separate experiments

differences (Figure 4f). The levels of pMLKL detected by immunoblot were also equivalent in lung lysates from *Sma*-infected TNFR1/2 KO mice and wild-type controls (Figure 4g). Together, these results rule out a requirement of TNFR signaling during *Sma* pneumonia and PFT-induced respiratory epithelial cell necroptosis.

As *Sma* carries lipopolysaccharide, the ligand for TLR4,[41] and recombinant pneumolysin has also been shown to bind to TLR4,[42] we also tested a role for TLR4 in PFT-induced necroptosis. Inhibition of TLR4 with the amino monosaccharide C34, which blocks TLR4 signaling by docking at the TLR4 receptor ligand site,[43] did not protect against *Sma*-, rPly- or α-toxin-induced death of A549 cells (Figure 5a). In normal human primary bronchial epithelial cells, modest but significant protection was observed against rPly but not *Sma* (Supplementary Figure 5). Similar to our results with TNFR1/2 KO mice, lung tissue and BALF from *Sma*-infected TLR4 KO mice showed no differences in bacterial load, LDH in BALF and albumin in the BALF *versus* controls (Figures 5b–e). Pathological analysis of tissues also showed no discernible differences between TLR4 KO and wild-type mice (Figure 5f). Finally, MLKL and pMLKL levels were not different between groups (Figure 5g). Based on these results, we conclude that PFTs induced respiratory epithelial cell death in a manner that is independent of TLR4.

PFT-induced lung epithelial cell necroptosis is the result of ion dysregulation. Ion dysregulation can occur as a result of PFT-mediated pore formation.[6] For this reason, we

explored whether membrane permeabilization and ion dysregulation induced activation of the necroptosis pathway in lung epithelial cells. The challenge of lungs cells with *Sma* or rPly resulted in increased intracellular Ca^{++} levels. The latter equivalent to levels seen in ionomycin-treated cells (Figure 6a). Briefly, ionomycin is an ionophore specific for Ca^{++}.[44] Further implicating an important role for ion dysregulation in the activation of necroptosis, necrostatin-5 protected against cell death induced by ionomycin and the ionophore nigericin (K^+), but not gramicidin (Na^+; Supplementary Figure 6a). Cell death caused by ionomycin and nigericin could also be blocked with Nec1s, GSK' 872 and necrosulfonamide, the respective inhibitors of RIP1, RIP3 and MLKL (Figure 6b). That necroptosis was activated in cells experiencing Ca^{++}, and K^+ dysregulation was verified by detection of pMLKL in ionomycin- and nigericin-challenged A549 cells using fluorescent microscopy (Figure 6c).

Directly implicating ion dysregulation following PFT exposure as an initiating signal for necroptosis, we observed that blocking cell membrane permeabilization with glycine[45] protected A549 cells from *Sma*- or rPly-induced death (Figure 6d). Moreover, cells in calcium-free media experienced reduced cell death following challenge with *Sma* or rPly (Figure 6e). Cell death was further diminished by the addition of potassium choloride to the calcium-free media, that in turn reduced K^+ efflux, in cells challenged with rPly (Figure 6e). Of note, no additional protective effect for Nec1s in rPly-challenged cells was observed in the absence of calcium or in media without calcium supplemented with potassium.
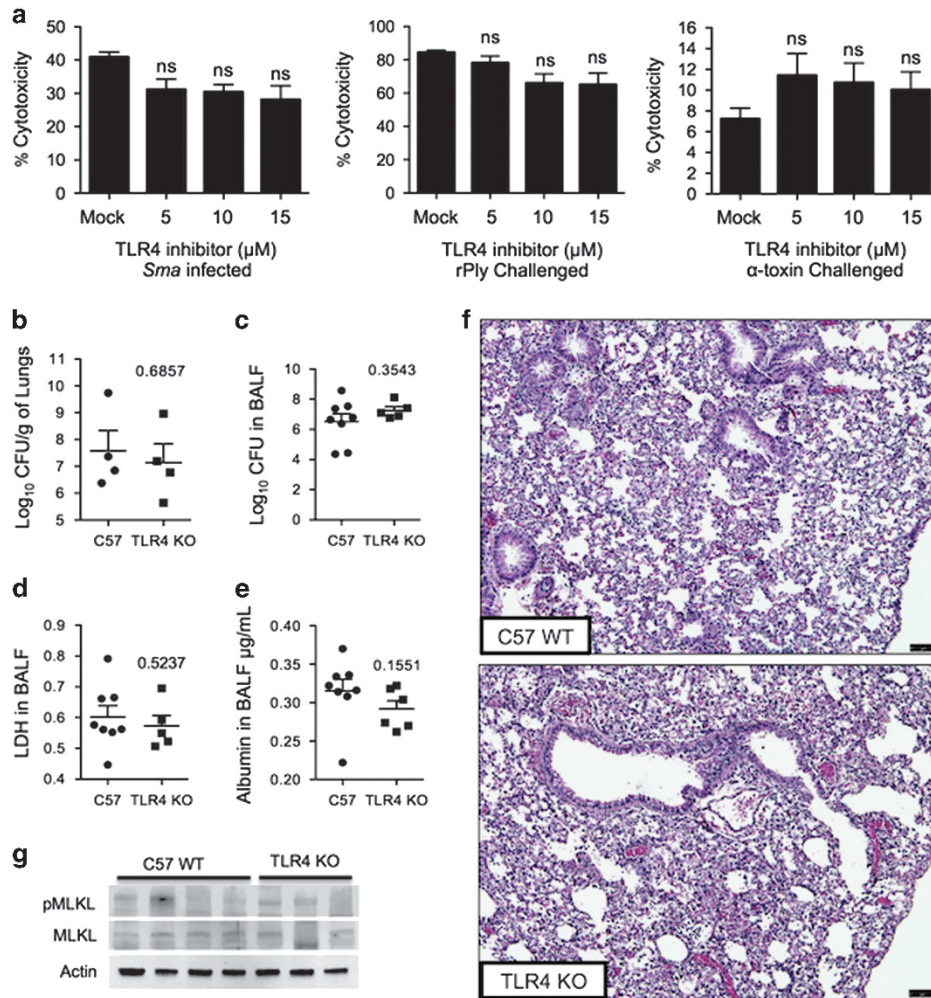
Figure 5 TLR4 inhibition does not protect against PFT-mediated respiratory epithelial cell necroptosis. (**a**) Percent cytotoxicity of A549 cells infected with *Sma* or challenged with either rPly or α-toxin pretreated with a selective inhibitor of TLR4 (C34) as determined using an LDH assay. (**b–g**) Six- to 8-week-old TLR4 KO mice and wild-type controls of the same age (four to seven mice per cohort) were infected intratracheally with *Sma*. After 24 h post-infection, levels of (**b**) bacterial titers in lungs and (**c**) BALF, (**d**) LDH and (**e**) albumin were determined. (**f**) H&E staining of lung tissue (scale bar represents 75 μm). (**g**) Immunoblots for pMLKL and MLKL in lung tissue. Mann–Whitney *U*-test was used for two-group comparisons. For multi-group comparisons, Dunn's multiple-comparison post-test was used: NS denotes no significance. The mean value for *in vitro* experiments was averaged from more than three separate experiments

Similarly, Nec1s only protected A549 cells treated with ionomycin when calcium was present in media (Supplementary Figure 6b). Finally and in cells challenged with rPly, cell membrane dissolution and levels of detectable pMLKL and pRIP3 was reduced or their activation delayed, respectively, when ion dysregulation was inhibited by the removal of Ca^{++} and addition of K^+ to the media (Supplementary Figures 7a and b). This observation corresponded to the changes in levels of intracellular calcium in rPly-challenged cells (Supplementary Figure 7c). Together, these results indicate a primary role for ion dysregulation during PFT-mediated activation of necroptosis.

Mitochondrial damage does not contribute to PFT-induced necroptosis. PFTs have also been implicated in causing mitochondrial damage.[46,47] Supporting this notion, we observed increased supernatant levels of cytochrome *C*

(Figure 7a), reduced levels of ATP (Figure 7b) and increased levels of cellular ROS (Figure 7c), after challenge with *Sma* or rPly. We also observed dispersal of J-aggregates (Figure 7d), a sign of mitochondrial membrane permeabilization and depolarization.[48] Inhibition of MLKL with necrosulfonamide diminished the release of cytochrome *C* and dispersal of J-aggregates in cells challenged with *Sma* or rPly (Figures 7e and d), indicating that necroptosis was contributing in some manner to mitochondrial damage. Recent studies have shown that RIP3 and Ca^{++} alterations due to ROS activate CamKII, which results in mitochondrial damage.[30,31] Ruling out a role for ROS-activated CamKII during PFT-induced necroptosis, pretreatment of A549 cells with the CamKII inhibitor KN-62 had no protective effect on cell death following challenge with *Sma* or rPly (Figure 7f). Moreover, blocking generation of mitochondrial derived ROS with TTFA, rotenone, antimycin (Figure 7g) and neutralization of cellular
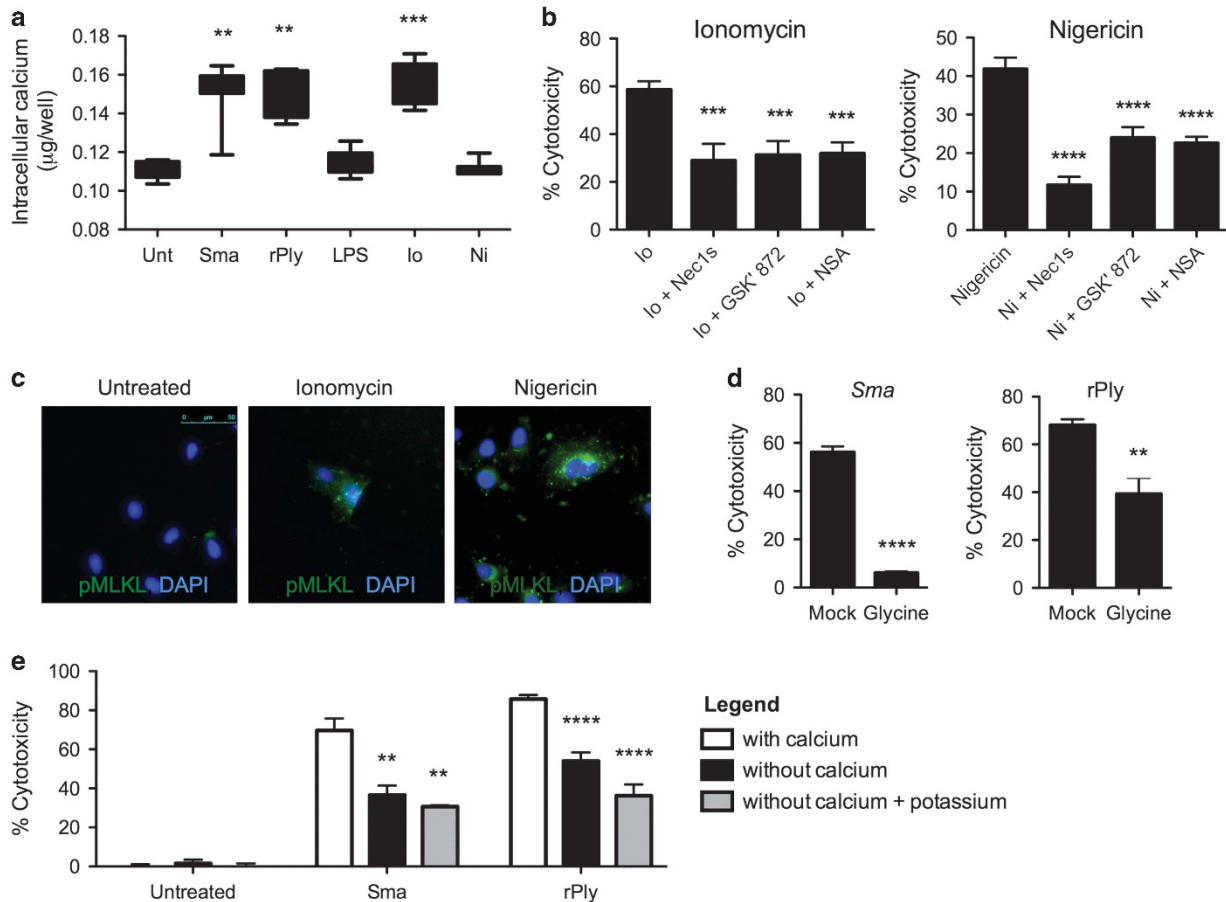
Figure 6 Ion dysregulation initiates respiratory epithelial cell necroptosis. (**a**) Intracellular calcium levels (μg/well) in A549 cells infected with *Sma* (MOI 10) or challenge with rPly (0.32 μg/ml), lipopolysaccharide (LPS, 1 μg/ml), ionomycin (Io, 20 μM), nigericin (Ni, 20 μM) or mock-treated. (**b**) Percent cytotoxicity of A549 alveolar epithelial cells pretreated with necrostatin-1 s (Nec1 s, 10 μM), the RIP3 inhibitor GSK' 872 (10 μM) and the MLKL inhibitor necrosulfonamide (NSA; 10 μM), then challenged with Io or Ni as determined using an LDH assay. (**c**) Immunofluorescent staining of Io- or Ni-challenged A549 cells. Cell nucleus (DAPI, blue), phosphorylated MLKL (pMLKL, green). (**d**) Percent cytotoxicity of A549 cells pretreated with glycine (10 μM), an inhibitor of membrane permeabilization, and challenged with *Sma* or rPly. (**e**) Percent cytotoxicity of A549 alveolar epithelial cells infected with *Sma* or challenged with rPly in the presence or absence of calcium in the culture media and calcium-depleted media supplemented with potassium. Mann–Whitney *U*-test was used for two-group comparisons. For multi-group comparisons, Dunn's multiple-comparison post-test was used: **$P \leqslant 0.01$, ***$P \leqslant 0.001$, ****$P \leqslant 0.0001$. The mean value for *in vitro* experiments was averaged from more than three separate experiments

ROS with DPI, catalase and *N*-acetylcysteine (Figure 7h) also had no effect on *Sma*-induced A549 cell death. Thus, mitochondrial damage is exacerbated by MLKL during PFT-induced necroptosis and this does not involve ROS or CamKII.

Pneumonia-induced respiratory tissue damage is mediated by RIP3-MLKL-dependent necroptosis. Finally, we sought to substantiate a detrimental role for lung epithelial cell necroptosis during pneumonia using genetic models. Mice deficient in RIP3 and MLKL had prolonged survival *versus* wild-type controls following intratracheal challenge with *Sma* (Figure 8a). RIP3 KO and MLKL KO mice infected with *Sma* had reduced number of erythrocytes and lower concentrations of albumin and LDH present in isolated BALF (Figures 8b, c, e and f), indicating preservation of the alveolar–capillary barrier. Hematoxylin and eosin (H&E)-stained lung sections from RIP3 KO and MLKL KO mice also showed diminished alveolar consolidation and edema as

compared with wild-type controls, this was particularly evident for MLKL KO mice (Figure 8h). No differences in bacterial titers in BALF of WT *versus* KO mice were observed at the time of killing (Figures 8d and g). The latter indicates that the observed differences in lung damage were mediated by the activation of necroptosis.

Discussion

Herein, we report that bacterial PFTs induce respiratory epithelial cell necroptosis and this requires RIP1, RIP3 and MLKL. Moreover, PFT-induced necroptosis is initiated in a manner that is independent of death receptor signaling. It is instead activated as a result of PFT-mediated membrane permeabilization. We show that mice and nonhuman primates experience necroptosis during severe pneumonia and report that blocking of necroptosis is beneficial to the respiratory tissue during bacterial infection. These findings firmly establish necroptosis as a key cell death pathway active
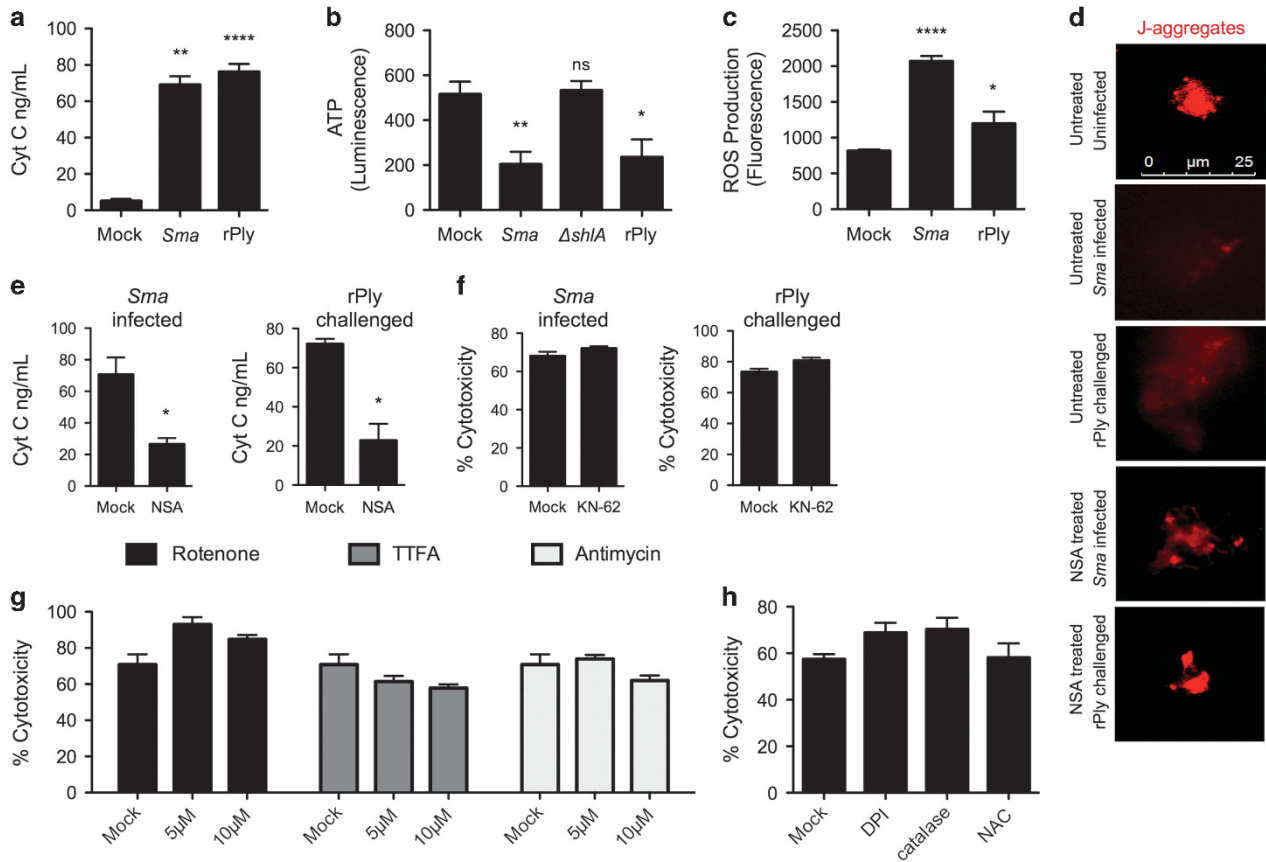
Figure 7 MLKL activity during PFT-induced necroptosis exacerbates mitochondrial damage. (**a**) Cytochrome *C* (ng/ml) levels in supernatants from A549 cells challenged with *Sma* or rPly. (**b**) ATP levels in cell pellets of A549 cells challenged with *Sma*, *ΔshlA* or rPly. (**c**) Reactive oxygen species levels in cell pellets of A549 cells challenged with *Sma* or rPly. (**d**) A549 cells pretreated with necrosulfonamide (NSA, 10 μM) were challenged with *Sma* or rPly. Mitochondrial permeabilization was visualized using a probe for J-aggregates (mitochondrial membrane potential dye, red). (**e**) Cytochrome *C* levels in supernatants from A549 cells, pretreated with necrosulfonamide (NSA, 10 μM) and challenged with *Sma* or rPly. (**f**) Percent cytotoxicity of *Sma*-infected or rPly-challenged A549 cells following pretreatment with CamKII inhibitor (KN-62, 10 μM) as determined using an LDH assay. (**g**) Percent cytotoxicity of *Sma*-infected A549 cells following pretreatment with rotenone (5 μM, 10 μM), 2-thenoyltrifluoroacetone (TTFA, 5 μM, 10 μM), antimycin (5 μM, 10 μM) or (**h**) diphenyleneiodonium (DPI, 10 μM), catalase (10 μM) or *N*-acetylcysteine (100 μM). Mann–Whitney *U*-test was used for two-group comparisons. For multi-group comparisons, Dunn's multiple-comparison post-test was used: *$P < 0.05$, **$P \leqslant 0.01$, ****$P \leqslant 0.0001$. The mean value for *in vitro* experiments was averaged from more than three separate experiments

during pneumonia, the eighth leading cause of death worldwide.[2]

Up to this point, the bulk of our knowledge on necroptosis came from studies that relied on cell death induced by the pro-inflammatory cytokine TNFα or following TLR engagement in the presence of a pan-caspase inhibitor.[18,25,49] Notably, our results showed that PFTs induce necroptosis independently of TNFR1, TNFR2 or TLR4 and without the chemical inhibition of caspases. We also rule out a role for CamKII-mediated mitochondrial damage. Our data demonstrates that it is instead ion dysregulation caused by PFT-mediated membrane permeabilization that leads to the activation of necroptosis during bacterial pneumonia. This was evidenced by the fact that necroptosis of lung cells could be initiated with ionophores specific for Ca^{++} and K$^+$; in addition, MLKL activation and PFT-mediated killing was abrogated when cells were in calcium-free media supplemented with potassium. These findings imply that necroptosis is either directly activated by ion dysregulation or that an intermediate and as-of-yet unknown molecule that acts as a sensor instead activates necroptosis.

Before this report, *in vitro* dysregulation of intracellular Ca^{++} levels has been shown to result in decreased ATP levels and induction of necrostatin-1 preventable death.[50,51] Our data solidify the notion that Ca^{++} and K$^+$ dysregulation by themselves are sufficient triggers to activate the necroptosis machinery leading to MLKL activation. MLKL then targets and exacerbates mitochondrial damage and this presumably explains the reduced ATP levels that are observed. With this view in mind, an expanded role for necroptosis can be speculated during diverse conditions where ion dysregulation occurs. One example being neurodegenerative diseases such as Alzheimer, Huntington's and Parkinson,[52,53] where it has been shown that annular protofibrils that resemble bacterial PFTs trigger cell death via ion dysregulation.[52] Studies investigating this possibility are now warranted.

Similar to PFT-induced necroptosis, how ion dysregulation activates pyroptosis is currently an open question. More specifically, it remains unknown how NLRP3 (i.e., cryopyrin) is activated by changes in K$^+$ concentrations. During pyroptosis, P2X7, Pannexin 1 and PFTs cause the efflux of K$^+$, which is
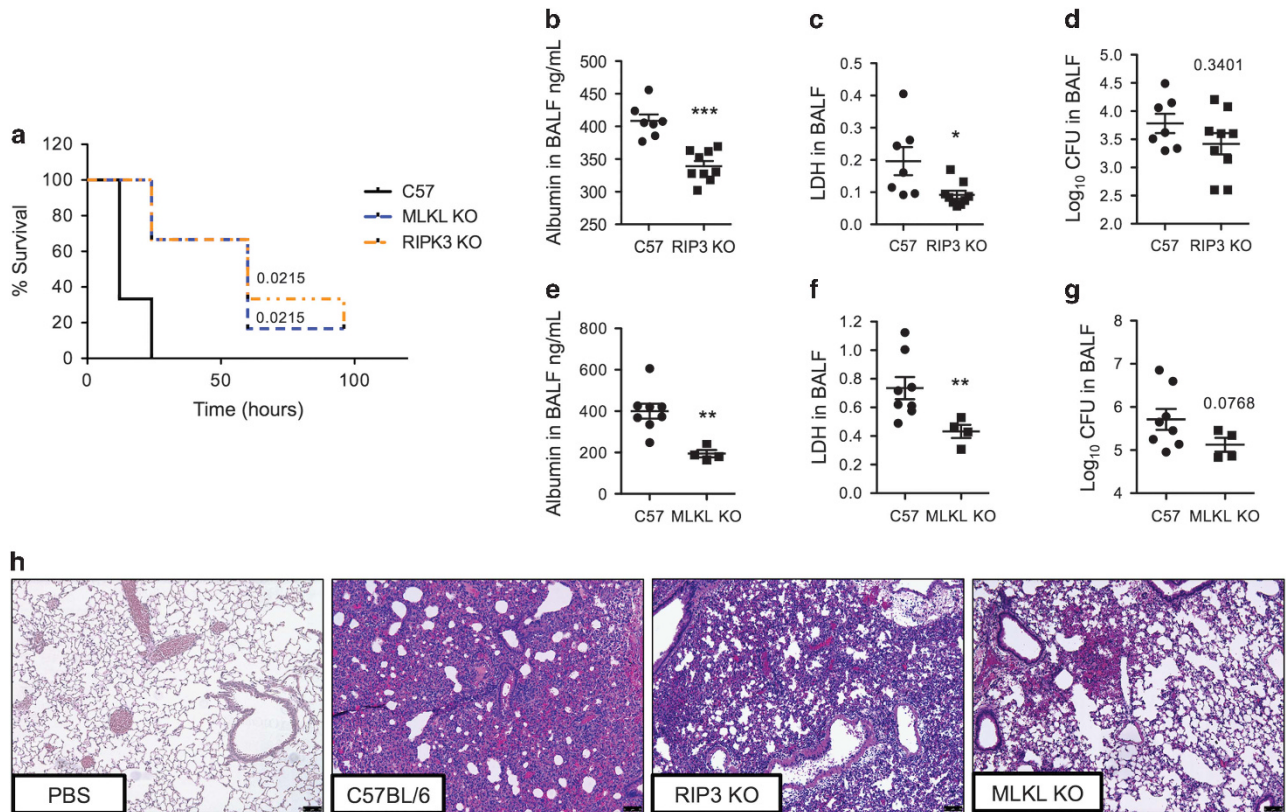
Figure 8 RIP3- and MLKL-deficient mice are protected against tissue damage and hemorrhage during *in vivo* bacterial pneumonia. (**a**) Survival of C57BL/6 MLKL KO mice, RIP3 KO mice and their respective wild-type controls (four to six mice per cohort) following a lethal dose of *Sma* (5×10^6 CFU) administered intratracheally. (**b–h**) C57BL/6 (**b–d, h**) RIP3 KO mice, (**e–h**) MLKL KO mice and their respective wild-type controls were infected intratracheally with *Sma* (four to nine mice per cohort). Twenty-four hours post infection, the levels of (**b** and **e**) albumin, (**c** and **f**) LDH and (**d** and **g**) bacterial titers in BALF were determined. (**h**) Representative images of H&E-stained lung tissue from above mice. Mann–Whitney *U*-test was used for two-group comparisons: *$P < 0.05$, **$P \leqslant 0.01$, ***$P \leqslant 0.001$. Log-rank Mantel–Cox test was used for survival curves

alone sufficient to activate the NLRP3 inflammasome and caspase-1. It is unknown whether NLRP3 directly senses K^+ efflux or whether another intermediate event or sensors trigger this mechanism.[54] In context of our findings herein, it is now also unclear as to how specificity in cell death pathway activation following ion dysregulation might be occurring. What leads to cell death by pyroptosis *versus* necroptosis during ion dysregulation? Perhaps intensity of signal or co-stimulation of a second receptor in a cell type-specific manner drives the decision process. Of note, both activation of caspase-1 or MLKL results in pore formation in the plasma membrane leading to further increases in K^+ efflux and Ca^{++} influx.[20,55] Thus ion dysregulation can be both an initiator and positive feedback mechanism for pyroptosis and necroptosis, both pro-inflammatory modes of cell death.

Necroptosis has been linked to the host defense during viral infections.[32,33,56–59] For example, during Influenza A infection *in vitro*, RIP3 activated parallel pathways of necroptosis and apoptosis and thereby eliminated infected cells. In the latter report, RIP3 KO mice, but not MLKL KO mice, experienced increased viral titers and elevated mortality when challenged with Influenza A, thereby suggesting that factors other than or in addition to MLKL driven membrane disruption were important for this protection.[32] In contrast to a protective role, our results unambiguously suggest PFT-mediated necroptosis

is detrimental to the host pulmonary epithelium during bacterial pneumonia. Our findings are complementary to those previously described for alveolar macrophages,[34,35] and strongly suggest that PFT-producing bacteria exploit necroptosis to enhance disease pathology and promote infection. Our results also suggest that necroptosis inhibition may be a viable adjunct therapy to antimicrobials in individuals experiencing severe bacterial infections.

In conclusion, we have described for the first time the occurrence of respiratory epithelial cell necroptosis during bacterial pneumonia. We show that ion dysregulation at the membrane level is responsible and that mitochondrial damage is exacerbated by the activation of MLKL. Our results expand on our molecular understanding of how PFTs kill and add to the body of evidence that blocking necroptosis is a way to protect against bacterial infection. We propose that PFTs are valuable tools to study necroptosis in cells without caspase inhibition.

Materials and Methods

Bacterial strains and growth conditions. A clinical isolate of *S. marcescens* (*Sma*) was obtained from Dr. James Jorgensen at the University of Texas Health Science Center at San Antonio, San Antonio, TX, USA. An isogenic, unmarked *shlA* deletion ($\Delta shlA$) was constructed by deleting the majority of the ShlA coding region (leaving behind the first five and the last five codons) via allelic

exchange as previously described.[8] *Sma* was grown on Luria-Bertani (LB) agar plates and incubated overnight at 30°C. A single colony was transferred to the LB broth and incubated overnight with rolling, then back diluted 1:50 for three additional hours, also at 30 °C. *Spn* serotype 4 strain TIGR4 wild-type and an isogenic pneumolysin-deficient mutant (Δ*ply*) were grown as previously described.[60] rPly was purified from transformed *E. coli* also as previously described.[60] *Listeria monocytogenes, Staphylococcus aureus,* uropathogenic *Escherichia coli,* were grown as previously described.[34] The inoculums were prepared by diluting the bacteria into sterile phosphate-buffered saline (PBS) to the final desired concentration (75 μl volume inoculum). The amount of colony-forming units (CFU) inoculated was confirmed at the time of infection by serial dilution of the inoculum, plating on agar plates and extrapolation from colony counts.

Mice and baboon infections. Female 6–8-week-old wild-type C57BL/6 mice and TNFR p55/p75 knockout (in a C57BL/6 background) from Jackson Laboratories (Sacramento, CA, USA) were used. MLKL and RIP3 knockout mice in the C57BL/6 background were obtained from Warren Alexander (Walter and Eliza Hall Institute of Medical Research Parkville, VIC, Australia) and Vishva Dixit (Genentech, San Francisco, CA, USA), respectively. TLR4 KO mice were obtained from Drs. Sue Michalek and Sadis Matalon (University of Alabama at Birmingham, Birmingham, AL, USA). Oropharyngeal aspiration was performed on each mouse as previously described.[8] Briefly, after being anesthetized (2% vaporized isoflurane), each mouse was hung upright by its incisors, the tongue gently pulled outward with blunt forceps and the respective inoculum pipetted into the oropharynx accompanied by coverage of the nares to achieve forced inhalation. All mice experiments were performed with a protocol (IACUC #20270) approved by the University of Alabama at Birmingham Institutional Animal Care and Use Committee and in agreement with the NIH Guide for the Care and Use of Laboratory Animals. Healthy baboons, with a median age 11 ratio years old (interquartile range: 10–19) were intrabronchially challenged with *Spn* (1×10^9 CFU) using a bronchoscope. During severe pneumonia (5–7 days after infection), the animals were killed and lung tissue was collected. All baboon experiments were performed using a protocol approved by the Southwest National Primate Research Center Institutional Animal Care and Use Committee and in agreement with the NIH Guide for the Care and Use of Laboratory Animals (IACUC #1443PC0).

Histology. After killing by pressurized CO_2 asphyxiation and pneumothorax, the lungs were inflated with 0.5 ml of optimal cutting temperature medium (Tissue-Tek OCT, Sakura, Torrance, CA, USA), surgically removed, transferred to molds, covered in OCT and snap-frozen. The tissue sections were stained with hematoxylin and eosin, or respective antibodies and reagents for immunofluorescence or immunohistochemistry (pMLKL, 1:1000 overnight, ab196436, Abcam, Cambridge, MA, USA). The images were captured using a Zeiss AxioXam MRm Rev3 and/or MRc cameras attached to a Zeiss AxioImager Z1 epifluorescent microscope (Carl Zeiss, Thornwood, NY, USA) or a Leica LMD6 with DFC3000G-1.3 megapixel monochrome camera (Leica Biosystems, Buffalo Grove, IL, USA).

BALF and cytospins. Using an 18-gauge Angiocath Autoguard catheter (Becton Dickinson, Sandy, UT, USA), we performed tracheotomies in killed mice as previously described.[8] Briefly, after the animals were tracheotomized, a three-way stopcock (Baxter, Deerfield, IL, USA) attached to two 3 ml syringes was used to wash lungs three times with 0.5 ml of PBS and collect BALF. BALF was then centrifuged and re-suspended in 0.5 ml PBS. Cell concentration was determined using the Cellometer Slide Chamber (Nexcelom Biosciences, Lawrence, MA, USA). Using a Cytospin 4 Centrifuge (Thermo Fisher Scientific, Suwanee, GA, USA), we fixed a concentration of 10^5 cells in 250 μl to Shandon CytoSpin-coated slides, following the manufacturer's instructions. The slides were stained for differentiation of blood cell types with Protocol Hema 3 stain set (Thermo Fisher Scientific), and inspected using microscopy (Carl Zeiss, ×10 magnification) for total number of PMNs and monocytes. For determination of bacterial burden in the lungs, BALF was serially diluted, plated and bacterial titers extrapolated from colony counts following overnight incubation.

Cell lines. A549 and LA-4 cells were grown in DMEM with 10% FBS and incubated at 37 °C with 5% CO_2. Normal human bronchial epithelial cells (NHBEC) were grown in bronchial epithelial cell basal medium supplemented with bronchial epithelial growth medium SingleQuots (Lonza, Allendale, NJ, USA) and incubated at 37 °C with 5% CO_2. For cytotoxicity assays, the cells were plated at a final concentration of 5×10^4 in 96-well plates and incubated as above.

Inhibitors and other chemicals. Necrostatin-1(#N9037), -5 (#N0164), -7 (#N3040), SPD304 (#S1697), C34 (#SML0832), Ionomycin (#I9657), Nigericin (#481990), Glycine (#410225), DPI (#300260), NAC (#A8199), rotenone (557368), antimycin (#A8674) and TTFA (#T27006) were obtained from Sigma-Aldrich (St. Louis, MO, USA). GSK' 872 (#2673) and Necrostatin-1 s (#2263) were obtained from BioVision (Milpitas, CA, USA). Necrosulfonamide (#5025) and R7050 (#5432) were obtained from Tocris Bioscience (Avonmouth, Bristol, UK). KN-62 (#sc-3560) was obtained from Santa Cruz (Dallas, TX, USA).

Silencing RNA. Commercially available siRNA targeting RIP3 (#61482) or MLKL (93430; Santa Cruz) were used to transfect A549 alveolar epithelial cells following the manufacturer's instructions.

***In vitro* infection of cells.** For *in vitro* studies, bacterial cells were grown as described above. After back dilution, bacteria was added to adherent mammalian cells at a multiplicity of infection (MOI) 10 for *S. marcescens* and 100 for *S. pneumoniae* in their respective media without phenol red+2% FBS for up to 4 h. For inhibition or protection experiments, cells were first pretreated with various concentrations of selected chemicals listed below for 1 h, and then exposed to bacteria, toxins or cytotoxic reagents. The concentration of rPly used has been previously shown to cause cardiomyocyte cytotoxicity[60] and 75% lysis in a hemolysis assay. In some instances, the cells were infected in DMEM media that lacked calcium and/or that had potassium chloride (130 mM) added.

Cell death assays. Cell death was evaluated by detection of the cytoplasmic enzyme lactate dehydrogenase (LDH) in the culture supernatants as previously described.[34] Briefly, the cells were spun down at $200 \times g$ for 5 min and 50 μl supernatant was removed from each well and passed to a new 96-well plate and immediately assayed for the presence of LDH using either the Cytotox 96 Assay kit (Promega, Madison, WI, USA) or Pierce LDH cytotoxicity kit (Thermo Fisher Scientific) according to the manufacturer's recommendations. Note that positive controls were treated with lysis buffer to liberate all cytoplasmic content approximately 30 min before supernatant harvest. 50 μl of reconstituted substrate solution was added to the supernatants, and then incubated for 30 min in the dark; the addition of 50 μl of stop solution provided by manufacturer terminated the reaction. The absorbance was measured at 490 nm in a BioTek Synergy H4 plate reader (BioTek, Winooski, VT, USA) or iMark Absorbance Microplate Reader (Bio-Rad Laboratories, Hercules, CA, USA).

ROS and ATP measurement. ROS concentration in cells was measured using the cell-permeant 2′,7′-dichlorodihydrofluorescein diacetate indicator of ROS (H2-DCF; Life Technologies, Carlsbad, CA, USA). ROS probe was added to each well to a final working concentration of ~ 5 mM, followed by a 30 min incubation at 37 °C. After incubation, a short recovery time of 15 m was allowed for cellular esterases to hydrolyze the acetoxymethyl ester or acetate groups. Fluorescence was measured with a fluorescent plate reader. ATP was measured using an ATP Assay Kit (Abcam). Cell culture supernatant was deproteinized using 10 kDa spin columns (Abcam). ATP standard curve and filtrate dilutions were combined with ATP reaction mix on a plate and incubated at room temperature for 30 min protected from light. Colorimetric output was measured with a microplate reader.

Immunoblots and quantification. Whole-cell extracts were prepared with RIPA buffer (150 mM NaCl, 1% NP-40, 0.5% DOC, 0.1% SDS and 50 mM TrisHCl) containing protease/phosphatase inhibitors (Pierce, Thermo Scientific, Waltham, MA, USA). The samples were run on TGX Stain-free polyacrylamide gels (Bio-Rad) by SDS-PAGE, under reducing conditions. Total protein was visualized before transfer on stain-free gels on a ChemiDoc XRS+ (Bio-Rad). Proteins were transferred onto nitrocellulose using a Trans-Blot Turbo Transfer System (Bio-Rad). Western blots were performed using standard methods and visualized using a Bio-Rad ChemiDoc XRS+ and Image Lab Software. The proteins from human cells were detected with antibodies against MLKL (3 μg/ml, ab118348, Abcam), pMLKL (1:1000, ab187091, Abcam), pRIP3 (1:1000, ab 209384, Abcam) and RIP3 (1:200, sc-7881, Santa Cruz). The mouse samples were detected with antibodies against MLKL (1:1000, ab172868, Abcam) and pMLKL (1:1000, ab196436, Abcam). Corresponding secondary antibody, horseradish peroxidase conjugated goat anti-rabbit or anti-mouse IgG, was used at 1:10 000 dilution (Jackson ImmunoResearch, West Grove, PA, USA). To confirm protein load, membranes were also probed with antibody against cytoskeletal actin at 1:5000 (Bethyl Laboratories Inc., Montgomery,

TX, USA). Image J was used to do densitometry analysis on protein blots. The protein levels were normalized to actin levels in the same sample.

ELISA. Albumin (Bethyl Laboratories Inc.) levels in BALF were measured using kits following the manufacturer's instruction. Calcium Detection (Colorimetric ELISA) was performed following the manufacturer's instructions (Abcam).

Mitochondrial depolarization assay. Mitochondrial membrane potential was visualized using MitoPT JC-1 dye (ImmunoChemistry, Bloomington, MN, USA) following the manufacturer's instructions.

Statistical analysis. Prism 5 (GraphPad Software, La Jolla, CA, USA) was used for graph development and statistical analysis. Survival curves were made using the Kaplan–Meier method and significance calculated using the log-rank test. Mann–Whitney U-tests were applied for two-group comparisons, and nonparametric ANOVA (Kruskal–Wallis) and Dunn's *post hoc* analysis were used for multiple-group comparisons.

Conflict of Interest

The authors declare no conflict of interest.

1. Ruuskanen O, Lahti E, Jennings LC, Murdoch DR. Viral pneumonia. *Lancet* 2011; **377**: 1264–1275.
2. Hoyert DL, Xu JQ. *Deaths: Preliminary Data for 2011*. National Center for Health Statistics: Hyattsville, MD, USA, 2012.
3. Alouf JE. Molecular features of the cytolytic pore-forming bacterial protein toxins. *Folia Microbiol* 2003; **48**: 5–16.
4. Gonzalez MR, Bischofberger M, Pernot L, van der Goot FG, Freche B. Bacterial pore-forming toxins: the (w)hole story? *Cell Mol Life Sci* 2008; **65**: 493–507.
5. Los FC, Randis TM, Aroian RV, Ratner AJ. Role of pore-forming toxins in bacterial infectious diseases. *Microbiol Mol Biol Rev* 2013; **77**: 173–207.
6. Dal Peraro M, Van Der Goot FG. Pore-forming toxins: ancient, but never really out of fashion. *Nat Rev Microbiol* 2016; **14**: 77–92.
7. Boyle-Vavra S, Daum RS. Community-acquired methicillin-resistant Staphylococcus aureus: the role of Panton–Valentine leukocidin. *Lab Invest* 2007; **87**: 3–9.
8. Gonzalez-Juarbe N, Mares CA, Hinojosa CA, Medina JL, Cantwell A, Dube PH *et al.* Requirement for *Serratia marcescens* cytolysin in a murine model of hemorrhagic pneumonia. *Infect Immun* 2015; **83**: 614–624.
9. Hirst R, Kadioglu A, O'callaghan C, Andrew P. The role of pneumolysin in pneumococcal pneumonia and meningitis. *Clin Exp Immunol* 2004; **138**: 195–201.
10. Inoshima I, Inoshima N, Wilke GA, Powers ME, Frank KM, Wang Y *et al.* A Staphylococcus aureus pore-forming toxin subverts the activity of ADAM10 to cause lethal infection in mice. *Nat Med* 2011; **17**: 1310–1314.
11. Labandeira-Rey M, Couzon F, Boisset S, Brown EL, Bes M, Benito Y *et al.* Staphylococcus aureus Panton-Valentine leukocidin causes necrotizing pneumonia. *Science* 2007; **315**: 1130–1133.
12. Neuhof H. Actions and interactions of mediator systems and mediators in the pathogenesis of ARDS and multiorgan failure. *Acta Anaesthesiol Scand* 1991; **35**: 7–14.
13. Vercammen D, Beyaert R, Denecker G, Goossens V, Van Loo G, Declercq W *et al.* Inhibition of caspases increases the sensitivity of L929 cells to necrosis mediated by tumor necrosis factor. *J Exp Med* 1998; **187**: 1477–1485.
14. Matsumura H, Shimizu Y, Ohsawa Y, Kawahara A, Uchiyama Y, Nagata S. Necrotic death pathway in Fas receptor signaling. *J Cell Biol* 2000; **151**: 1247–1256.
15. Holler N, Zaru R, Micheau O, Thome M, Attinger A, Valitutti S *et al.* Fas triggers an alternative, caspase-8-independent cell death pathway using the kinase RIP as effector molecule. *Nat Immunol* 2000; **1**: 489–495.
16. Smith CC, Davidson SM, Lim SY, Simpkin JC, Hothersall JS, Yellon DM. Necrostatin: a potentially novel cardioprotective agent? *Cardiovasc Drugs Ther* 2007; **21**: 227–233.
17. Pasparakis M, Vandenabeele P. Necroptosis and its role in inflammation. *Nature* 2015; **517**: 311–320.
18. Newton K, Manning G. Necroptosis and inflammation. *Annu Rev Biochem* 2016; **85**: 743–763.
19. Micheau O, Tschopp J. Induction of TNF receptor I-mediated apoptosis via two sequential signaling complexes. *Cell* 2003; **114**: 181–190.
20. Cai Z, Jitkaew S, Zhao J, Chiang H-C, Choksi S, Liu J *et al.* Plasma membrane translocation of trimerized MLKL protein is required for TNF-induced necroptosis. *Nat Cell Biol* 2014; **16**: 55–65.
21. Hildebrand JM, Tanzer MC, Lucet IS, Young SN, Spall SK, Sharma P *et al.* Activation of the pseudokinase MLKL unleashes the four-helix bundle domain to induce membrane localization and necroptotic cell death. *Proc Natl Acad Sci USA* 2014; **111**: 15072–15077.
22. Murphy JM, Czabotar PE, Hildebrand JM, Lucet IS, Zhang J-G, Alvarez-Diaz S *et al.* The pseudokinase MLKL mediates necroptosis via a molecular switch mechanism. *Immunity* 2013; **39**: 443–453.
23. Su L, Quade B, Wang H, Sun L, Wang X, Rizo J. A plug release mechanism for membrane permeation by MLKL. *Structure* 2014; **22**: 1489–1500.
24. Wang H, Sun L, Su L, Rizo J, Liu L, Wang L-F *et al.* Mixed lineage kinase domain-like protein MLKL causes necrotic membrane disruption upon phosphorylation by RIP3. *Mol Cell* 2014; **54**: 133–146.
25. He S, Liang Y, Shao F, Wang X. Toll-like receptors activate programmed necrosis in macrophages through a receptor-interacting kinase-3–mediated pathway. *Proc Natl Acad Sci USA* 2011; **108**: 20054–20059.
26. Kaiser WJ, Sridharan H, Huang C, Mandal P, Upton JW, Gough PJ *et al.* Toll-like receptor 3-mediated necrosis via TRIF, RIP3, and MLKL. *J Biol Chem* 2013; **288**: 31268–31279.
27. Wu J, Huang Z, Ren J, Zhang Z, He P, Li Y *et al.* Mlkl knockout mice demonstrate the indispensable role of Mlkl in necroptosis. *Cell Res* 2013; **23**: 994–1006.
28. Kuriakose T, Man SM, Malireddi RS, Karki R, Kesavardhana S, Place DE *et al.* ZBP1/DAI is an innate sensor of influenza virus triggering the NLRP3 inflammasome and programmed cell death pathways. *Sci Immunol* 2016; **1**: aag2045.
29. Thapa RJ, Ingram JP, Ragan KB, Nogusa S, Boyd DF, Benitez AA *et al.* DAI senses influenza A virus genomic RNA and activates RIPK3-dependent cell death. *Cell Host Microbe* 2016; **20**: 674–681.
30. Zhang T, Zhang Y, Cui M, Jin L, Wang Y, Lv F *et al.* CaMKII is a RIP3 substrate mediating ischemia-and oxidative stress-induced myocardial necroptosis. *Nat Med* 2016; **22**: 175–182.
31. Luczak ED, Anderson ME. CaMKII oxidative activation and the pathogenesis of cardiac disease. *J Mol Cell Cardiol* 2014; **73**: 112–116.
32. Nogusa S, Thapa RJ, Dillon CP, Liedmann S, Oguin TH, Ingram JP *et al.* RIPK3 activates parallel pathways of MLKL-driven necroptosis and FADD-mediated apoptosis to protect against influenza A virus. *Cell Host Microbe* 2016; **20**: 13–24.
33. Mocarski ES, Guo H, Kaiser WJ. Necroptosis: the Trojan horse in cell autonomous antiviral host defense. *Virology* 2015; **479–480**: 160–166.
34. Gonzalez-Juarbe N, Gilley RP, Hinojosa CA, Bradley KM, Kamei A, Gao G *et al.* Pore-forming toxins induce macrophage necroptosis during acute bacterial pneumonia. *PLoS Pathog* 2015; **11**: e1005337.
35. Kitur K, Parker D, Nieto P, Ahn DS, Cohen TS, Chung S *et al.* Toxin-induced necroptosis is a major mechanism of Staphylococcus aureus lung damage. *PLoS Pathog* 2015; **11**: e1004820.
36. Mitchell TJ, Dalziel CE. The biology of pneumolysin. In: Anderluh G, Gilbert R (eds). *MACPF/CDC Proteins - Agents of Defence, Attack and Invasion Dordrecht.* Springer: The Netherlands, 2014, pp 145–160.
37. Bartlett JG. Diagnostic test for etiologic agents of community-acquired pneumonia. *Infect Dis Clin North Am* 2004; **18**: 809–827.
38. Mandell LA, Wunderink RG, Anzueto A, Bartlett JG, Campbell GD, Dean NC *et al.* Infectious Diseases Society of America/American Thoracic Society consensus guidelines on the management of community-acquired pneumonia in adults. *Clin Infect Dis* 2007; **44**: S27–S72.
39. He MM, Smith AS, Oslob JD, Flanagan WM, Braisted AC, Whitty A *et al.* Small-molecule inhibition of TNF-α. *Science* 2005; **310**: 1022–1025.
40. King MD, Alleyne CH Jr, Dhandapani KM. TNF-alpha receptor antagonist, R-7050, improves neurological outcomes following intracerebral hemorrhage in mice. *Neurosci Lett* 2013; **542**: 92–96.
41. Beutler B. Tlr4: central component of the sole mammalian LPS sensor. *Curr Opin Immunol* 2000; **12**: 20–26.
42. Malley R, Henneke P, Morse SC, Cieslewicz MJ, Lipsitch M, Thompson CM *et al.* Recognition of pneumolysin by Toll-like receptor 4 confers resistance to pneumococcal infection. *Proc Natl Acad Sci USA* 2003; **100**: 1966–1971.
43. Neal MD, Jia H, Eyer B, Good M, Guerriero CJ, Sodhi CP *et al.* Discovery and validation of a new class of small molecule Toll-like receptor 4 (TLR4) inhibitors. *PLoS ONE* 2013; **8**: e65779.
44. Caridha D, Yourick D, Cabezas M, Wolf L, Hudson T, Dow G. Mefloquine-induced disruption of calcium homeostasis in mammalian cells is similar to that induced by ionomycin. *Antimicrob Agents Chemother* 2008; **52**: 684–693.
45. Brennan MA, Cookson BT. Salmonella induces macrophage death by caspase-1-dependent necrosis. *Mol Microbiol* 2000; **38**: 31–40.
46. Bischofberger M, Gonzalez MR, van der Goot FG. Membrane injury by pore-forming proteins. *Curr Opin Cell Biol* 2009; **21**: 589–595.

47. Braun JS, Hoffmann O, Schickhaus M, Freyer D, Dagand E, Bermpohl D *et al*. Pneumolysin causes neuronal cell death through mitochondrial damage. *Infect Immun* 2007; **75**: 4245–4254.

48. Xu SY, Hu YF, Li WP, Wu YM, Ji Z, Wang SN *et al*. Intermittent hypothermia is neuroprotective in an *in vitro* model of ischemic stroke. *Int J Biol Sci* 2014; **10**: 873–881.

49. Liu X, Shi F, Li Y, Yu X, Peng S, Li W *et al*. Post-translational modifications as key regulators of TNF-induced necroptosis. *Cell Death Dis* 2016; **7**: e2293.

50. Nomura M, Ueno A, Saga K, Fukuzawa M, Kaneda Y. Accumulation of cytosolic calcium induces necroptotic cell death in human neuroblastoma. *Cancer Res* 2014; **74**: 1056–1066.

51. Xu X, Chua CC, Kong J, Kostrzewa RM, Kumaraguru U, Hamdy RC *et al*. Necrostatin-1 protects against glutamate-induced glutathione depletion and caspase-independent cell death in HT-22 cells. *J Neurochem* 2007; **103**: 2004–2014.

52. Kagan BL, Hirakura Y, Azimov R, Azimova R. The channel hypothesis of Huntington's disease. *Brain Res Bull* 2001; **56**: 281–284.

53. Lashuel HA, Hartley D, Petre BM, Walz T, Lansbury PT Jr. Neurodegenerative disease: amyloid pores from pathogenic mutations. *Nature* 2002; **418**: 291.

54. Broz P, Dixit VM. Inflammasomes: mechanism of assembly, regulation and signalling. *Nat Rev Immunol* 2016; **16**: 407–420.

55. Jorgensen I, Miao EA. Pyroptotic cell death defends against intracellular pathogens. *Immunol Rev* 2015; **265**: 130–142.

56. Chien H, Dix RD. Evidence for multiple cell death pathways during development of experimental cytomegalovirus retinitis in mice with retrovirus-induced immunosuppression: apoptosis, necroptosis, and pyroptosis. *J Virol* 2012; **86**: 10961–10978.

57. Guo H, Kaiser WJ, Mocarski ES. Manipulation of apoptosis and necroptosis signaling by herpesviruses. *Med Microbiol Immunol* 2015; **204**: 439–448.

58. Omoto S, Guo H, Talekar GR, Roback L, Kaiser WJ, Mocarski ES. Suppression of RIP3-dependent necroptosis by human cytomegalovirus. *J Biol Chem* 2015; **290**: 11635–11648.

59. Wang W, Wang W-H, Azadzoi KM, Su N, Dai P, Sun J *et al*. Activation of innate antiviral immune response via double-stranded RNA-dependent RLR receptor-mediated necroptosis. *Sci Rep* 2016; **6**: 22550.

60. Brown AO, Mann B, Gao G, Hankins JS, Humann J, Giardina J *et al*. Streptococcus pneumoniae translocates into the myocardium and forms unique microlesions that disrupt cardiac function. *PLoS Pathog* 2014; **10**: e1004383.